2011-05

Influence of crystal field potential on the spectroscopic parameters of SiO2.B2O3.PbO glass doped with Nd2O3

Journal of Luminescence, Amsterdam : Elsevier, v. 131, n. 5, p. 1029-1036, May 2011
http://www.producao.usp.br/handle/BDPI/49718

Journal of Luminescence 131 (2011) 1029–1036

Contents lists available at ScienceDirect

Journal of Luminescence

journal homepage: www.elsevier.com/locate/jlumin

Influence of crystal field potential on the spectroscopic parameters of $SiO_2 \cdot B_2O_3 \cdot PbO$ glass doped with Nd_2O_3

N.O. Dantas [a], E.O. Serqueira [a], M.J.V. Bell [b,*], V. Anjos [b], E.A. Carvalho [b], S.A. Lourenço [c], M.A. Pereira-da-Silva [d,e]

[a] Laboratório de Novos Materiais Isolantes e Semicondutores (LNMIS), Instituto de Física, Universidade Federal de Uberlândia, CP593, 38400-902, Uberlândia—MG, Brazil
[b] Laboratório de Espectroscopia de Materiais, Departamento de Física, Universidade Federal de Juiz de Fora, Juiz de Fora-MG, 36036-330, Brazil
[c] Universidade Tecnológica Federal do Paraná—Campus Apucarana, 86812-460, Apucarana—PR, Brazil
[d] Instituto de Física de São Carlos, USP, São Carlos, SP 13560-250, Brazil
[e] Centro Universitário Central Paulista, UNICEP, São Carlos, SP 13563-470, Brazil

ARTICLE INFO

Article history:
Received 13 October 2010
Received in revised form
2 January 2011
Accepted 24 January 2011
Available online 4 February 2011

Keywords:
Glasses
Nanoparticles
Raman
Luminescence
Nd^{3+}
Judd–Ofelt theory

ABSTRACT

This paper presents the optical characteristics of Nd^{3+} silicate glass (SiO_2–B_2O_3–PbO), synthesized by the fusion method. Two sets of samples were prepared: glass and corresponding glass ceramics. Optical absorption, luminescence, Raman spectroscopy and atomic force microscopy (AFM) measurements were performed in order to determine the structural properties of the systems and the radiative characteristics of Nd^{3+} ions. Near infrared luminescence exhibited typical Nd^{3+} bands. Raman and AFM measurements indicated nanocrystal growth with thermal treatment of the glass ceramics. Judd–Ofelt calculations also confirmed that heat treatment induced structural rearrangement of the samples that was dependent on Nd_2O_3 concentration. This resulted in changes in the optical and physical properties of the samples, including stimulated emission cross section and rigidity.

1. Introduction

The optical properties of rare-earth-doped dielectric solids have been extensively investigated [1–4]. In particular, the use of rare-earth (RE) ions emitting in the optical-fiber spectral range has attracted considerable interest in luminescent material applications [5,6]. Due to their potential applications in efficient lasing and frequency upconversion processes, the investigation of optimized doped systems merits substantial effort. In this respect, one successful approach is to obtain glass ceramics by controlled heat treatment of glass precursors. It has been demonstrated that this procedure improves the mechanical, thermal, electrical and optical properties of a system. In this way, glass ceramics combine the mechanical and optical properties of glass with the crystal-like environment of rare earth ions. The composite material allows control of the chemical environment of the RE ion and reduces clustering and consequent luminescence quenching.

SiO_2–B_2O_3–PbO (SBP) glasses present high transparence in the optical window, including the NIR region. In addition, the phonon energy is relatively low due to the presence of high atomic mass elements such as Pb. Phonons play a very important role in Nd-doped glasses, since the higher the phonon energy, the lower the radiative emission. In this sense, the glass composition is evaluated considering the phonon energies of the components [7].

This paper reports on the optical properties of Nd^{3+} ions in SBP glass and glass ceramics. Atomic force microscopy and Raman scattering measurements demonstrated that thermal annealing induced structural rearrangement of the samples, which modified the radiative properties of Nd^{3+}. These results were reinforced by Judd–Ofelt calculations.

The Judd–Ofelt (JO) theory [8,9] has been widely used to study the environment surrounding RE ions in glass [10–15]. The theory gives the Judd–Ofelt parameters Ω_2, Ω_4 and Ω_6, from which radiative properties can be obtained. Ω_2 is related to the RE – O ligand field asymmetry of the host matrix such that as Ω_2 increases, symmetry decreases and covalency increases [16,17]. Ω_6 represents the degree of Ln – O covalency such that decreases in Ω_6 are associated with high covalency. Ω_4 is related to "long range" structural interaction like viscosity at high temperatures and ionic packing density at low temperatures [12,13].

2. Theory

The Judd–Ofelt theory [8,9] was used to calculate the radiative rates of Nd^{3+} ions in the SBP host in the near infrared spectral

* Corresponding author.
E-mail address: mjbell@fisica.ufjf.br (M.J.V. Bell).

0022-2313/$ - see front matter © 2011 Elsevier B.V. All rights reserved.
doi:10.1016/j.jlumin.2011.01.017

region. This required the calculation of electric dipole oscillator strength, P_{ed}, as follows:

$$P_{ed} = \frac{8\pi^2 mc}{3h}\frac{v}{2J+1}\chi\sum_{\lambda=2,4,6}\Omega_\lambda\left|\left\langle f^N\psi_J\right|U^{(\lambda)}\left|f^N\psi_{J'}\right\rangle\right|^2 \quad (1)$$

where $\chi=(n^2+2)^2/9n$ is the local field correction factor, m is the electron mass, v is the frequency (in cm^{-1}), c is the speed of light, J is the total angular momentum of the initial state, h is the Planck constant, n is the refractive index, $U^{(\lambda)}$ is the tensor operator of rank λ given by Carnall et al. [18] and f^N is the wave function of states with N electrons in the 4f shell with total angular momentum J. Finally, Ω_λ represent the Judd–Ofelt parameters. Magnetic-dipole oscillator strength (P_{md}) is currently considered host independent, and values from the literature can be used [19]. Experimental oscillator strength (P_{exp}) is given by $P_{exp}=P_{ed}+P_{md}$, where the electric dipole and/or quadrupole oscillator strengths are not considered [20]. Judd–Ofelt parameters Ω_λ are obtained by the least-square method and oscillator strengths for any transitions are calculated by Eq. (1):

Radiative transition rates (A) are obtained from the usual expression:

$$A(aJ,bJ') = \frac{64\pi^4 e^2}{3h}\frac{v^3}{(2J+1)}\chi\sum_{\lambda=2,4,6}\Omega_\lambda\left|\left\langle f^N\psi_J\right|U^{(\lambda)}\left|f^N\psi_{J'}\right\rangle\right|^2 \quad (2)$$

Radiative lifetime is given by

$$\tau(^{2S+1}L_J\rightarrow{}^{2S'+1}L_{J'}) = \frac{1}{\sum_{J'}A(^{2S+1}L_J\rightarrow{}^{2S'+1}L_{J'})} \quad (3)$$

Once radiative rates are known, branching ratios (β) of the near infrared emissions may be calculated by

$$\beta(^{2S+1}L_J\rightarrow{}^{2S'+1}L_{J'}) = \frac{A(^{2S+1}L_J\rightarrow{}^{2S'+1}L_{J'})}{\sum_{J'}A(^{2S+1}L_J\rightarrow{}^{2S'+1}L_{J'})} \quad (4)$$

where the summation in Eq. (4) encompasses all the final states.

3. Experimental set-up

The optical absorption and luminescence experiments reported in this study were carried out using single Nd^{3+}-doped lead silicate glass with the following composition: $SiO_2\cdot B_2O_3\cdot PbO$ (mol%). All Nd concentrations are expressed in wt% with values of 0.5, 1.0, 1.5, 2.0, 2.5, 3.0, 3.5, 4.0, 4.5 and 5.0. The mixture was melted in an aluminum crucible at 1400 °C for 30 min and then quenched to room temperature. To release thermal stress, samples were annealed at 350 °C for 2 h. The melt was manually rotated at least three times inside the crucible. This procedure has shown to be efficient since the homogeneity of the samples, tested by absorption measurements at different points of the samples, shows the same optical density. Crystallization was induced in a second group of samples by exposing them to 500 °C for 120 h. Therefore, two sample groups were created: glass (G) and glass ceramics (GC) treated at 500 °C.

Finally, the samples were cut and polished for optical measurements. Optical absorption (OA) spectra were obtained using a Shimadzu UV 3600 spectrophotometer operating in the range of 175–3300 nm. The samples were optically excited using a 514.5 nm argon-ion laser line. Luminescence spectra were recorded using a SPEX-750M monochromator equipped with an InGaAs detector. Raman measurements were performed with a T64000 Horiba Jobin Yvon spectrometer coupled to a N_2 liquid refrigerated CCD detector and excited by a He–Ne laser (632,8 nm and 15 mW). Resolutions of the Raman and luminescence spectra were 4 cm^{-1} and 1 nm, respectively. Absorption measurements were recorded with 2 nm resolution.

A Shimadzu DTA-50 (accurate to ±5 °C) was used to determine the physical characteristics of the glasses, including glass transition (T_g) and maximum crystallization (T_c) temperatures. The differential thermal analysis (DTA) measurements were performed in an atmosphere of nitrogen gas using samples of approximately 50 mg with grains ranging in diameter from 0.085 to 0.180 mm, and heating at a rate of 20 °C/min.

The atomic force microscopy (AFM) images were obtained with a Multimode Nanoscope IIIa (Digital Instruments – Veeco).

4. Results and discussion

Fig. 1 shows the DTA of undoped SBP glass. The crystallization and vitreous transition temperatures are 504 and 463 °C, respectively. Based on such results, the temperature of 500 °C was chosen to the subsequent thermal treatments during 120 h in order to verify the effect of crystallization on the optical parameters of Nd^{3+} ions. The DTA also indicates that the SBP matrix does not present the crystallization peak, as for example the LBA matrix [21].

Fig. 2 shows AFM images of the glass and glass ceramic. No crystallization is observed in the case of glass (Fig. 2a), while the glass ceramics (120 h heat treatment at 500 °C) indicate the presence of nanocrystals averaging 50 nm (Fig. 2b).

Fig. 3 exhibits the Raman spectra of SBP in glassy region (Fig. 3a) and corresponding glass ceramic structure (Fig. 3b). The spectrum of the vitreous matrix treated at 350 °C shows broad bands centered at 520, 750 and 1400 cm^{-1}. These bands could be associated with the presence of Si–O–Si and borate stretching vibrations [22]. Specifically, the broad band between 1250 and 1500 cm^{-1} can be assigned to B–O stretching in the chain-type metaborate groups. The component centered at around 1410 cm^{-1} is associated with BO_3 units bonding to BO_4 units, while the one at about 1480 cm^{-1} is assigned to BO_3 bonding to BO_3 units. The band at 1510 cm^{-1} is related to BO_3 units in boroxil rings, and the band at around 1320 cm^{-1} to "loose" BO_3 units [22]. The band centered at 3300 cm^{-1} is attributed to the presence of PbO in the glass matrix [23], and the small bands between 550 and 650 cm^{-1} are attributed to Si–O–Si rocking [24]. The SBP glasses have inhomogeneous structure with crystallites detected by the Raman spectrum exhibited in Fig. 3b. Raman spectra similar to the one shown in Fig. 3a were also recorded in all samples (not shown). The Raman spectrum shown in Fig. 3b was found after several spatial scans inside the samples, with resolution of 100 nm. This suggests that the concentration of such crystallites is very low. In fact, the concentration of the nanoparticles is so low that XRD

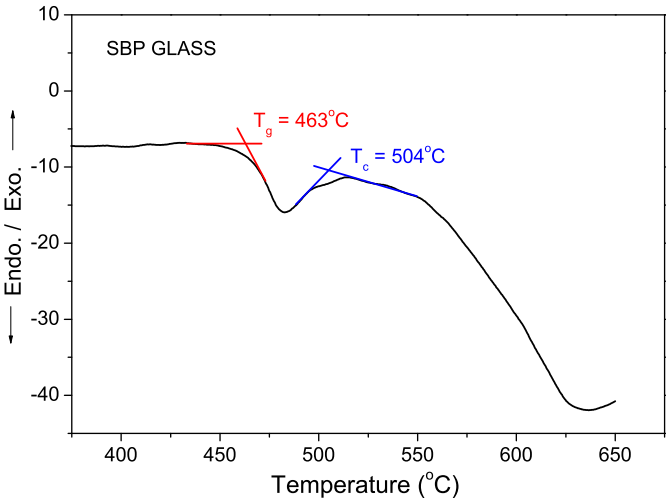

Fig. 1. DTA results for undoped SBP glass, treated at 350 °C during 24 h. T_g and T_c are 463 and 503 °C, respectively.

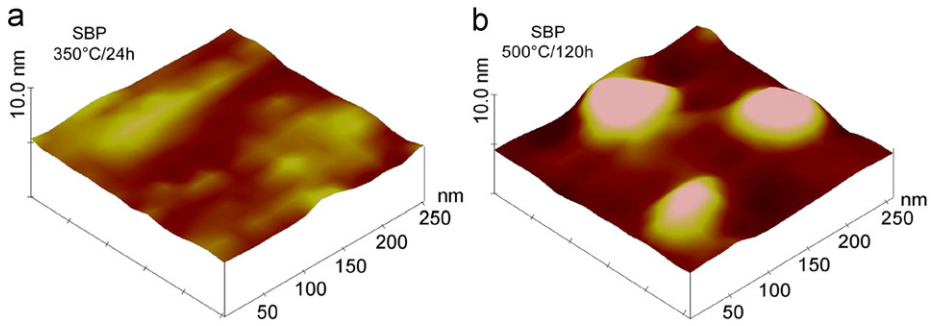

Fig. 2. AFM images of (a) SBP glass (350 °C for 24 h) and (b) SBP glass–ceramic (350 °C for 24 h+500 °C during 120 h) .

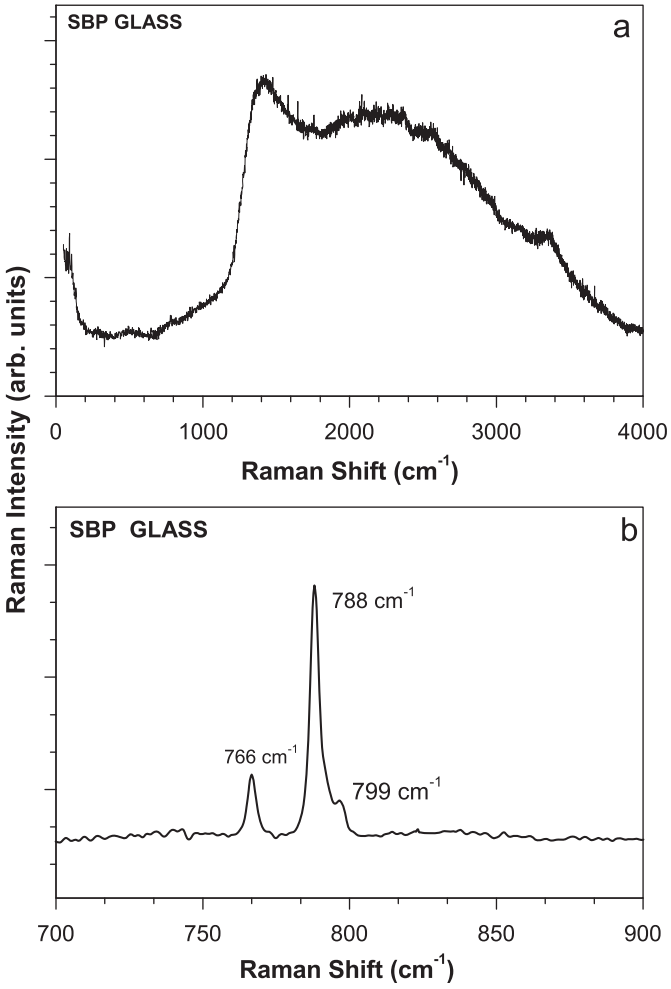

Fig. 3. Raman spectra of SBP glass+350 °C (24 h) in (a) glassy region and (b) crystalline region.

technique was not sensitive and only the amorphous nature of the SBP glass was identified.

The nanoparticle Raman spectrum is assigned to that of cristobalite, which is usually observed in the crystallization processes of borosilicate glass [25,26]. The Raman peaks in Fig. 3b, which are centered at 766, 788, 796 cm^{-1} are characteristic of crystallite from α and β cristobalite [25]. Nevertheless one should be aware that we are dealing with nanoparticles, which may alter the bulk crystal structure and, therefore, the phonons dispersion and the respective oscillator strengths. A more thorough study of this subject will be addressed in the future.

Fig. 4 shows the optical absorption coefficient of the SBP+$X$$Nd_2O_3$ (wt%) glass and glass ceramic samples. It is apparent that these bands were not modified by variation in Nd_2O_3 concentration (i.e. increasing concentrations of Nd_2O_3 did not result in changes to the energy positions of the ion levels). On the other hand, comparisons of glass and glass ceramic samples show slight changes in the lineshape of the Nd^{3+} emissions. This can be explained by assuming that, unlike glass, glass ceramics undergo atomic rearrangement, which results in crystal field modification [27]. Given this, it is expected that the spectroscopic parameters would be different and that the glass ceramic formation process could make the material more efficient for optical device applications.

Tables 1 and 2 show the experimental and calculated oscillator strengths of Nd^{3+} ions embedded in the SBP glass and glass ceramic samples, depending on concentration. It can be seen that oscillator strength tends to decrease when samples are heat treated. This may be related to a tendency towards crystallization (i.e. structural rearrangement leads to reduced inter-atomic interactions by occupying positions of lower energy).

Fig. 5 shows Ω_2 of the SBP+$X$$Nd_2O_3$ (wt%) glass and glass ceramic samples. It can be seen that these parameters increase with increase in concentrations of Nd^{3+}. Thus, these ion concentrations help to change the surrounding geometry, which leads to reductions in symmetry. It was also observed that covalency increases with concentration. As symmetry reduces, covalent bonds increase between ions in the sample, matrix and dopants. It should also be noted that for fixed concentrations, Ω_2 decreases when the samples are heat treated. This confirms that thermal treatment at 500 °C can crystallize the SPB glass matrix doped with Nd_2O_3. This effect is more pronounced for concentrations of about $1.5Nd_2O_3$ (wt%).

Fig. 6 shows the Judd–Ofelt intensity parameter Ω_4 for the SBP+$X$$Nd_2O_3$ (wt%) glass and glass ceramic samples. It can be seen that the glass samples have a minimum Ω_4 value of about $2.0Nd_2O_3$ (wt%), while the glass ceramic is just starting to grow. It can also be observed that the range of Ω_4 is greater for the glass samples than for the glass ceramic.

Fig. 7 shows the Ω_6 Judd–Ofelt intensity parameter for the SBP+$X$$Nd_2O_3$ (wt%) glass and ceramic–glass samples. It should be noted that the behavior of Ω_6 for the glass samples is similar to that of the glass ceramic, but with a greater range of values.

In this study, Ω_2 increases with increase in Nd_2O_3 concentrations. In other words, the ligand field around the Nd^{3+} ion becomes more asymmetric as the concentration of this ion increases. At the same time, the Nd – O covalent bond seems to increase suggesting that the Nd – O bond becomes less ionic. This can be seen in Fig. 8, which shows the $1/\Omega_6$ values. Ionic bonds are less directional than covalent bonds, which is in agreement with a decrease in symmetry or an increase in Ω_2.

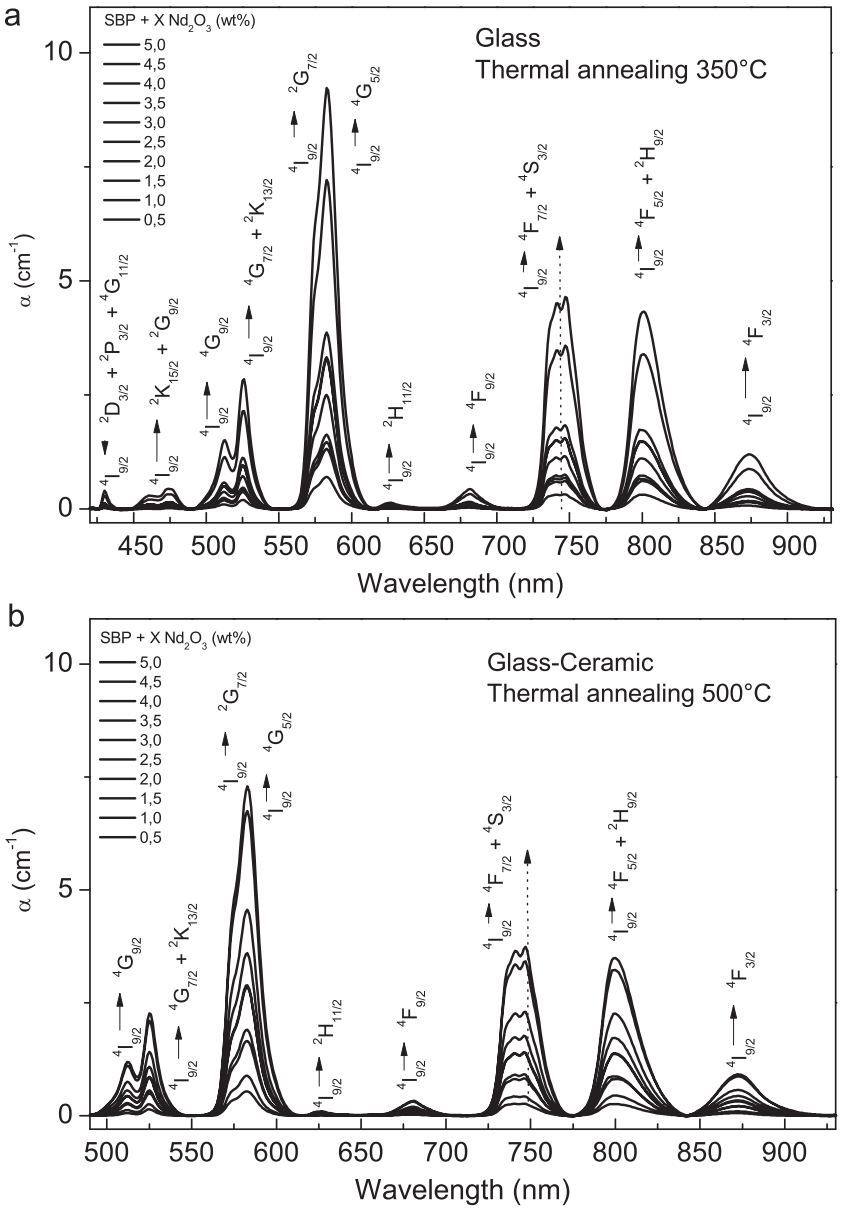

Fig. 4. Optical absorption coefficients of the (a) glass and (b) glass–ceramic SBP+XNd$_2$O$_3$ (wt%) samples. The vertical dotted line indicates the increase in Nd concentration.

Table 1
Experimental (f_{exp}) and calculated (f_{cal}) oscillator strength of Nd^{3+} transitions in SBP glass as a function of concentration ($f \times 10^{-6}$ and $N \times 10^{20}$ ions/cm^3).

N (wt%)	N (ions/cm^3)	874 nm ($^4I_{9/2} \rightarrow {}^4F_{3/2}$)		800 nm ($^4I_{9/2} \rightarrow {}^4F_{5/2}+{}^4H_{9/2}$)		747 nm ($^4I_{9/2} \rightarrow {}^4F_{7/2}+{}^4S_{3/2}$)		681 nm ($^4I_{9/2} \rightarrow {}^4F_{9/2}$)		626 nm ($^4I_{9/2} \rightarrow {}^4H_{11/2}$)		583 nm ($^4I_{9/2} \rightarrow {}^4G_{7/2}+{}^4G_{5/2}$)		525 nm ($^4I_{9/2} \rightarrow {}^4G_{7/2}+{}^2K_{13/2}$)		512 nm ($^4I_{9/2} \rightarrow {}^4G_{9/2}$)		475 nm ($^2K_{15/2} \rightarrow {}^2G_{9/2}$)		430 nm ($^4I_{9/2} \rightarrow {}^2D_{3/2}+{}^2P_{3/2}+{}^4G_{11/2}$)	
		f_{exp}	f_{cal}	f_{exp}	f_{cal}	f_{exp}	f_{cal}	f_{exp}	f_{cal}	f_{exp}	f_{cal}	f_{exp}	f_{cal}	f_{exp}	f_{cal}	f_{exp}	f_{cal}	f_{exp}	f_{cal}	f_{exp}	f_{cal}
0.5	0.614	0.667	0.760	2.327	2.395	2.428	2.412	0.279	0.181	0.147	0.053	8.037	8.050	1.687	1.487	1.125	0.505	0.441	0.414	0.138	0.202
1.0	1.346	0.424	0.488	1.420	1.430	1.379	1.389	0.134	0.106	0.069	0.031	4.789	4.796	1.012	0.909	0.627	0.313	0.254	0.255	0.072	0.133
1.5	2.071	0.344	0.389	1.181	1.187	1.170	1.179	0.136	0.089	0.045	0.026	3.946	3.950	0.804	0.742	0.481	0.254	0.215	0.208	0.056	0.105
2.0	2.717	0.319	0.357	1.167	1.185	1.224	1.224	0.136	0.090	0.037	0.026	3.762	3.767	0.776	0.708	0.469	0.243	0.217	0.200	0.053	0.093
2.5	3.493	0.271	0.302	1.098	1.138	1.251	1.236	0.134	0.089	0.031	0.026	3.578	3.584	0.741	0.651	0.448	0.219	0.224	0.182	0.051	0.074
3.0	4.136	0.323	0.353	1.303	1.344	1.483	1.467	0.150	0.105	0.032	0.031	4.042	4.047	0.838	0.753	0.498	0.257	0.268	0.214	0.063	0.085
3.5	4.857	0.414	0.449	1.613	1.674	1.836	1.808	0.141	0.130	0.027	0.038	5.010	5.019	1.082	0.941	0.618	0.323	0.305	0.268	0.064	0.110
4.0	5.493	0.495	0.523	1.900	1.972	2.184	2.150	0.210	0.154	0.048	0.045	5.656	5.663	1.185	1.088	0.716	0.377	0.412	0.315	0.100	0.127
4.5	5.933	0.681	0.683	2.453	2.617	2.966	2.872	0.261	0.205	0.071	0.060	7.566	7.576	1.628	1.440	0.960	0.497	0.559	0.417	0.144	0.164
5.0	6.523	0.866	0.885	2.974	3.167	3.496	3.389	0.317	0.245	0.112	0.072	9.182	9.196	2.022	1.783	1.209	0.621	0.734	0.519	0.195	0.221

Table 2
Experimental (f_{exp}) and calculated (f_{cal}) oscillator strength of Nd^{3+} transitions in SBP glass–ceramic as a function of concentration ($f \times 10^{-6}$ and $N \times 10^{20}$ ions/cm^3).

N (wt%)	N (ions/cm^3)	873 nm ($^4I_{9/2} \rightarrow {}^4F_{3/2}$)		800 nm ($^4I_{9/2} \rightarrow {}^4F_{5/2} + {}^4H_{9/2}$)		746 nm ($^4I_{9/2} \rightarrow {}^4F_{7/2} + {}^4S_{3/2}$)		681 nm ($^4I_{9/2} \rightarrow {}^4F_{9/2}$)		626 nm ($^4I_{9/2} \rightarrow {}^4H_{11/2}$)		583 nm ($^4I_{9/2} \rightarrow {}^4G_{7/2} + {}^4G_{5/2}$)		525 nm ($^4I_{9/2} \rightarrow {}^4G_{7/2} + {}^2K_{13/2}$)		512 nm ($^4I_{9/2} \rightarrow {}^4G_{9/2}$)	
		f_{exp}	f_{cal}	f_{exp}	f_{cal}	f_{exp}	f_{cal}	f_{exp}	f_{cal}	f_{exp}	f_{cal}	f_{exp}	f_{cal}	f_{exp}	f_{cal}	f_{exp}	f_{cal}
0.5	0.735	0.319	0.356	1.643	1.570	1.752	1.805	0.173	0.126	0.026	0.037	4.302	4.297	0.716	0.812	0.322	0.280
1.0	1.519	0.262	0.338	1.374	1.306	1.384	1.441	0.119	0.103	0.026	0.030	3.480	3.481	0.682	0.696	0.410	0.246
1.5	2.056	0.310	0.366	1.399	1.362	1.447	1.481	0.127	0.106	0.027	0.031	3.714	3.715	0.735	0.741	0.447	0.261
2.0	2.709	0.334	0.391	1.504	1.475	1.584	1.613	0.127	0.115	0.027	0.034	3.974	3.976	0.798	0.796	0.505	0.281
2.5	3.402	0.360	0.399	1.451	1.454	1.563	1.569	0.133	0.113	0.028	0.033	3.935	3.938	0.816	0.795	0.526	0.282
3.0	4.099	0.373	0.416	1.520	1.530	1.652	1.656	0.143	0.119	0.031	0.035	4.256	4.260	0.885	0.842	0.561	0.296
3.5	4.552	0.444	0.476	1.692	1.733	1.885	1.868	0.157	0.135	0.034	0.039	4.798	4.803	1.022	0.956	0.648	0.336
4.0	5.316	0.496	0.539	1.886	1.941	2.110	2.086	0.170	0.151	0.040	0.044	5.252	5.259	1.168	1.065	0.767	0.378
4.5	5.852	0.560	0.599	2.127	2.207	2.431	2.392	0.202	0.172	0.051	0.050	6.106	6.115	1.354	1.212	0.854	0.426
5.0	6.182	0.658	0.691	2.497	2.624	2.940	2.873	0.239	0.206	0.061	0.060	7.303	7.316	1.637	1.430	1.012	0.499

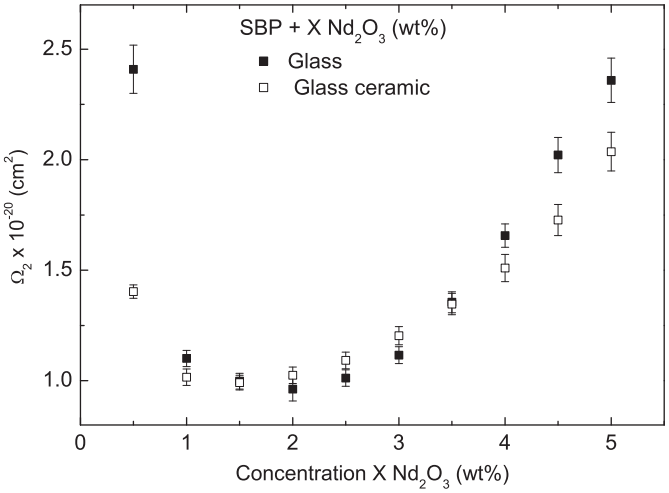

Fig. 5. Judd–Ofelt intensity parameter, Ω_2, for the SBP+XNd$_2$O$_3$ (wt%) glass and glass–ceramic samples.

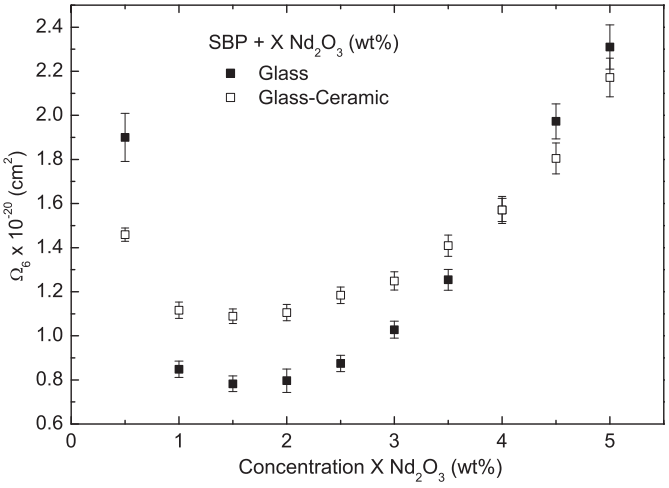

Fig. 7. Judd–Ofelt intensity parameter, Ω_6, for the SBP+XNd$_2$O$_3$ (wt%) glass and glass–ceramic samples.

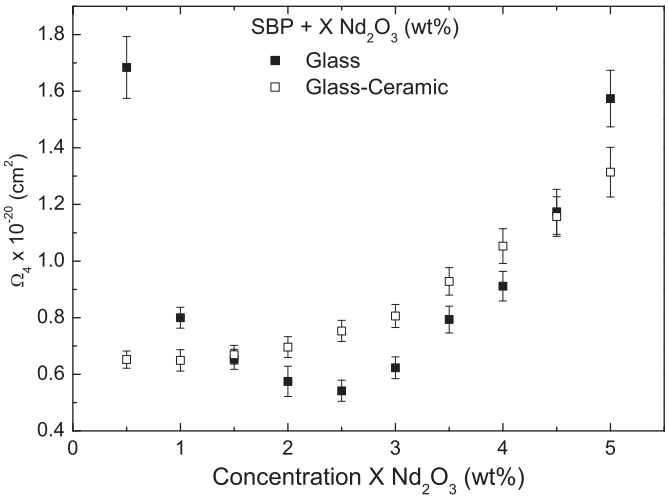

Fig. 6. Judd–Ofelt intensity parameter, Ω_4, for the SBP+XNd$_2$O$_3$ (wt%) glass and glass–ceramic samples.

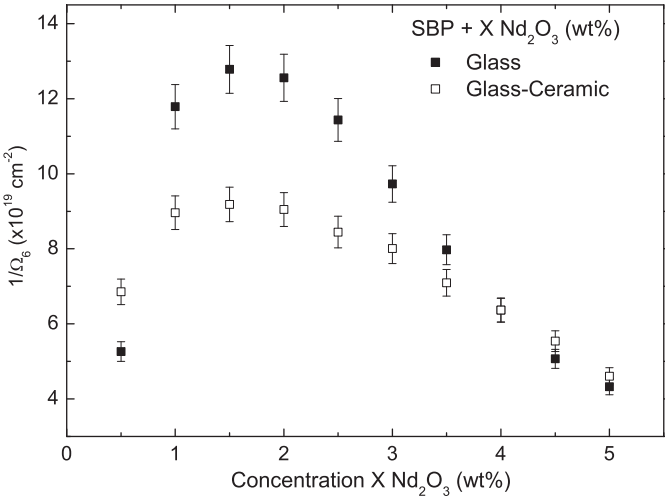

Fig. 8. Inverse of Ω_6 for the SBP+XNd$_2$O$_3$ (wt%) glass and glass–ceramic samples that correspond to reductions in ionicity in relation to Ω_2, which increases covalency.

The degree of ionic bonding [28] can be determined from the electric dipole moment of a molecule. For example, if a hypothetical molecule, AB, were purely ionic, the positive charge center would be in the A^+ ion and the negative charge center would be in the B^- ion. In this case, the electric dipole moment of the module would be given by $p_{ion}=er_o$, where r_o is the equilibrium separation between the two ions. Therefore, the dipole moment would be $p_{ion}=e\ r_o=(1.6\times 10^{-19}\ \text{C})(2.36\times 10^{-10}\ \text{m})=3.78\times 10^{-29}\ \text{C m}$. The experimental

electric dipole moment would be $p_{exp}=300\times10^{-29}$ C m. When a molecule is purely covalent the dipole moment is zero. Thus, one can define the degree of ionic bonding as a ratio of p_{exp} to p_{ion}. In this case, 3.00/3.78=0.79.

Furthermore, increases in Ω_4 with increase in concentrations of Nd_2O_3 indicate possible far-reaching effects on the host matrix in the area surrounding Nd−O such as increased glass packing density [11,12]. Increased Ω_4, in turn, suggests that more Nd^{3+} ions are dissolved in the glass matrix. This is credited to the association of Ω_4 with repulsive long range interactions between the cations [11–13].

Another possibility would be that repulsive forces could have existed between Nd and other adjacent cations, thus modifying other cations. Modifying the cation network did not result in Nd^{3+} and Na^+ sharing the same oxygen bridge [29]. Thus, Nd increased the repulsive force of Nd cations towards neighbors of Na cations, which, if present, could have also contributed to increases in Ω_4.

The Ω_6 parameter, on the other hand, is proportional to the rigidity of the host [30]. The literature shows that NdF_3 based samples present an increase in transitions from glass to glass ceramics, which implies an improvement in mechanical properties [31]. In this study, Fig. 9 shows the ratio between the Ω_6 values for the glass and glass ceramic samples with a minimum of about $1.5Nd_2O_3$ (wt%). In other words, the system would have low rigidity for low concentrations and high rigidity (glass system) for high concentrations.

Jacobs and Weber [32] have reported that the Ω_4/Ω_6 ratio could be considered as the spectroscopic quality factor for classifying glass matrices. The $^4F_{3/2}\rightarrow{}^4I_{11/2}$ emission intensity can be classified by the ratio Ω_4/Ω_6. The lowest value of the most intense laser transition is typically about 0.76–0.95 for oxide and fluoro-oxide glass [33,34]. The results for the NdF_3 based samples were relatively low and decreased further to 0.71 after heat treatment. A relatively low value, 0.69, was also obtained for the Nd_2O_3 based glass ceramic. However, relatively high values were obtained for Nd^{3+} in solution [31]. The values obtained from glass and glass ceramic samples considered in this study are shown in Fig. 10. It can be seen that this factor decreases as the concentration for the glass and the glass ceramic samples increases. This may be explained by assuming that, to have the same crystallization effect, the temperature of the heat treatment is dependent on the concentration of the dopant. Thus the higher concentrations tend to the same value of (Ω_4/Ω_6). For lower concentrations, thermal treatment promotes atom rearrangement and consequent alterations to the Ω_4/Ω_6 ratio.

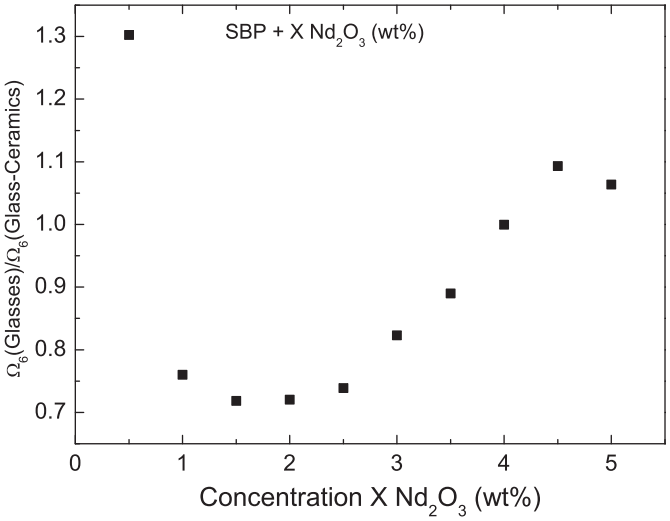

Fig. 9. Ratio of Ω_6 values for glass and glass–ceramic samples.

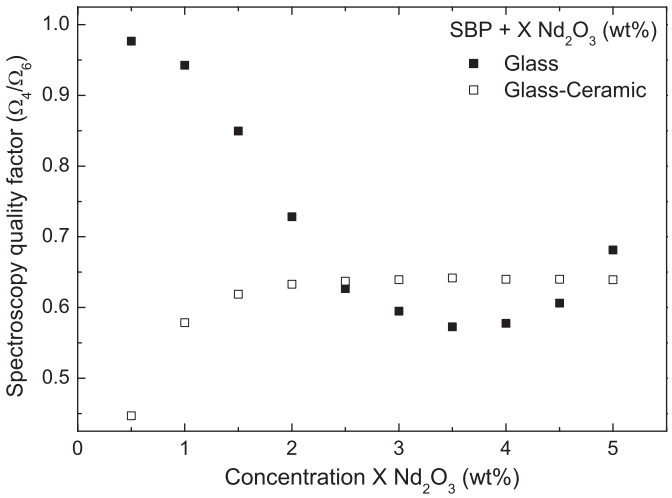

Fig. 10. Spectroscopic quality factors of the SBP+$X$$Nd_2O_3$ (wt%) glass and glass–ceramic samples.

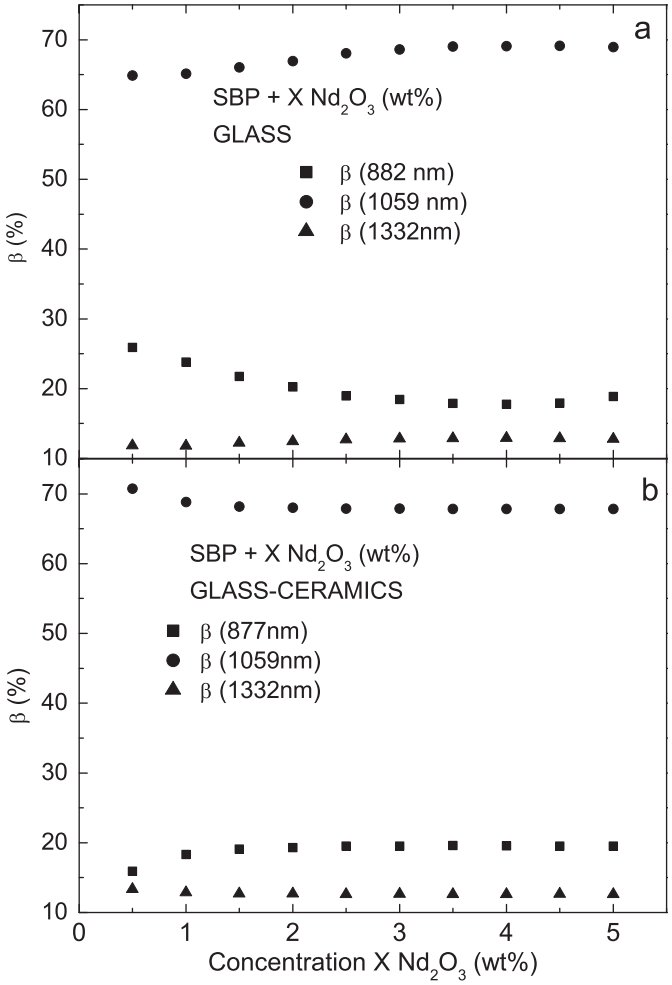

Fig. 11. Emission branching ratio from the $^4F_{3/2}$ state for $^4I_{9/2,\ 11/2,\ 13/2}$ for the SBP+$X$$Nd_2O_3$ (wt%) glass and glass–ceramic samples.

Fig. 11 shows the branching ratio β of the $^4F_{3/2}$ state for $^4I_{9/2,\ 11/2,\ 13/2}$ of the SBP+$X$$Nd_2O_3$ (wt%) glass (Fig. 11a) and glass ceramic (Fig. 11b) samples. Notice that variation in β is more pronounced for

the $^4F_{3/2} \rightarrow {}^4I_{9/2}$ and $^4F_{3/2} \rightarrow {}^4I_{11/2}$ transitions. It can be seen that as the concentration of Nd_2O_3 increases, the $^4F_{3/2} \rightarrow {}^4I_{9/2}$ transition decreases and the $^4F_{3/2} \rightarrow {}^4I_{11/2}$ transition increases moderately. However, the opposite occurs for the glass ceramic samples where heat treatment produces structural rearrangement, which modifies optical properties for low concentrations of Nd_2O_3. For high concentrations, heat treatment does not produce the same result and transition rates remain unchanged.

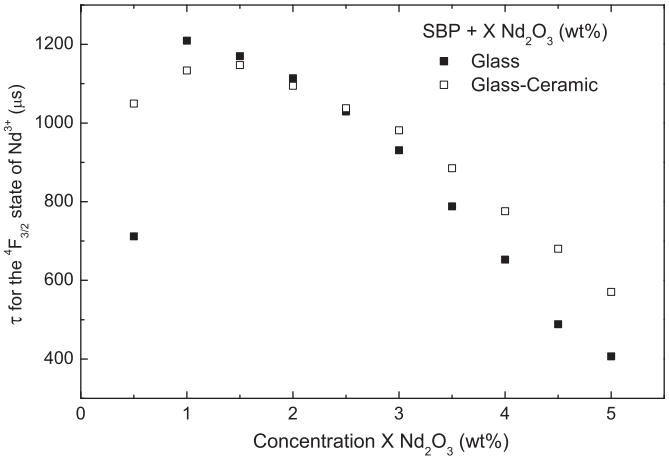

Fig. 12. Radiative lifetime for the $^4F_{3/2}$ state of Nd^{3+} ions in SBP+XNd$_2$O$_3$ (wt%) glass and glass–ceramic samples.

Fig. 12 shows the Radiative Lifetime of the SBP+XNd$_2$O$_3$ (wt%) glass and ceramic–glass samples. It is known that ion–ion interactions can decrease the lifetime of the state responsible for relaxation emissions, in this case $^4F_{3/2}$. While with heat treatment, it was possible to lower the rate of radiative lifetime reduction from 1200 to 400 μs for glass samples and from 1150 to 600 μs for glass ceramic samples.

The stimulated emission cross section is also favored by low values of effective linewidth, $\Delta\lambda_{eff}$ [31]. In other words, the lower the effective linewidth, the greater the stimulated emission. This can be seen in Fig. 13 where the $^4F_{3/2} \rightarrow {}^4I_{11/2}$ transition results in lower values for both glass and glass ceramics. It can be seen that heat treatment helped to decrease effective linewidth, which can be explained by assuming that spontaneous emission depends on dipole interaction, which could be higher in a disordered system than in a corresponding ceramic–glass system. Once rearrangement occurs in this system, the interaction tends to decrease and thereby reduce the spontaneous emission cross section and, most significantly, the stimulated emission cross section.

The stimulated emission cross section is obtained with the help of the Fuchtbauer–Ladenburg equation [35,36]:

$$\sigma(aJ,bJ') = \frac{\lambda_p^4}{8\pi cn^2 \Delta\lambda_{eff}} A(aJ,bJ') \quad (5)$$

where λ_p is the emission wavelength (cm), A is the transition probability obtained from Judd–Ofelt and $\Delta\lambda_{eff}$ is the effective linewidth of the emission band obtained from the following

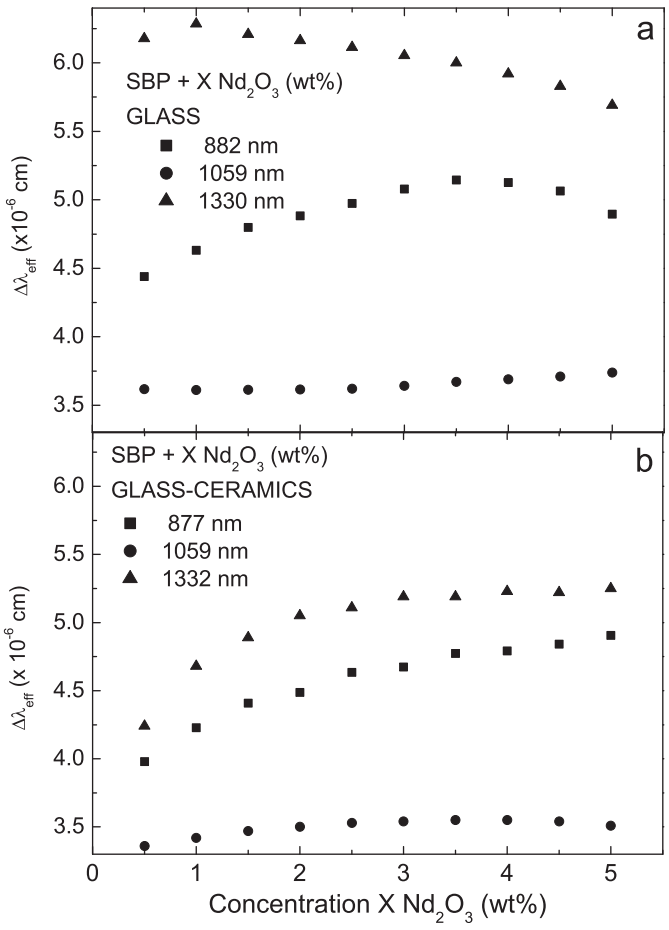

Fig. 13. Effective linewidth for the SBP+XNd$_2$O$_3$ (wt%) glass and glass–ceramic samples.

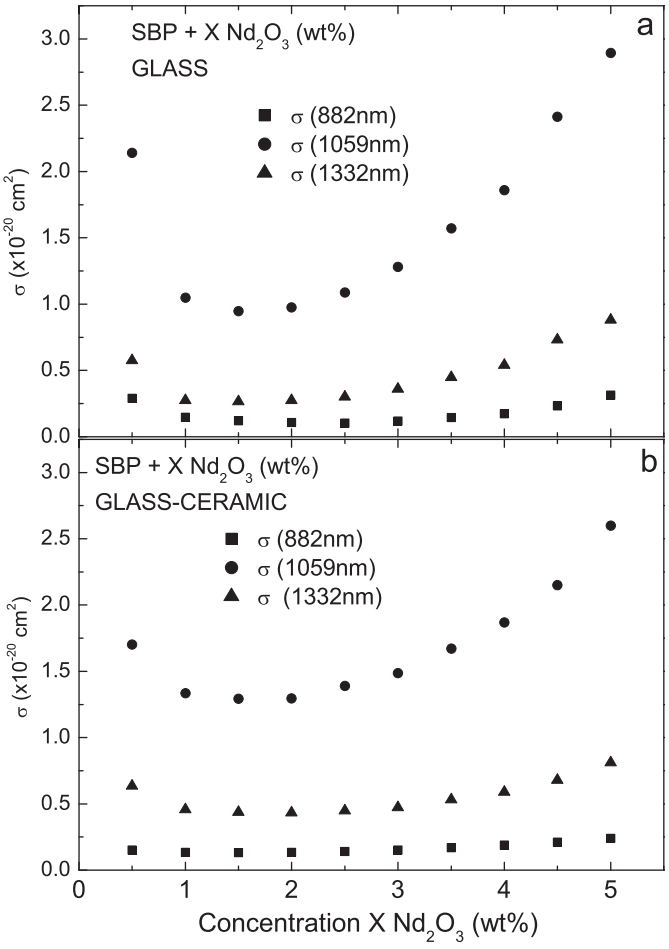

Fig. 14. Effective emission cross section for the SBP+XNd$_2$O$_3$ (wt%) glass and glass–ceramic samples.

expression:

$$\Delta\lambda_{eff} = \frac{\int I(\lambda)d\lambda}{I(\lambda_p)} \quad (6)$$

where the integral is over the entire emission band and I_p is the peak emission intensity.

For comparison, the values of σ for the NdF_3 based glass (σ_G) and glass–ceramic (σ_{GC}) are $\sigma_G = 4{,}68 \times 10^{-20}$ cm^2 and $\sigma_{GC} = 6{,}88 \times 10^{-20}$ cm^2 [31]. In this study σ was calculated as shown in Fig. 14.

Fig. 14 shows that increase in the concentration of Nd_2O_3 results in enhancement of stimulated emission cross section. Accordingly, it appears that the stimulated emission cross section increased with heat treatment for low concentration samples where crystallization was more pronounced.

5. Conclusion

Nd^{3+}-doped lead borosilicate glass (SiO_2–B_2O_3–PbO) samples were synthesized by fusion. Their optical properties were investigated by means of optical absorption and luminescence. Raman and AFM measurements were also performed in order to investigate the structure of the glass and glass ceramics. Judd–Ofelt parameters were calculated and oscillator strength, radiative rates, radiative lifetimes, branching ratios, effective linewidths and stimulated emission cross sections were obtained.

Heat treatment can induce crystallization effects that depend on RE ion concentration and thereby alter optical properties, increase stimulated emission cross section and moderate declines in radiative lifetime as a function of concentration. Heat treatment can also modify physical properties because as ionicity decreases, covalency tends to increase, which results in increased sample rigidity. We believe that these results may inspire further investigation of these systems in a search for device applications.

Acknowledgments

The authors acknowledge the financial support from the Brazilian agencies CNPq, FAPEMIG and CAPES. Special acknowledgment goes to S. Watanabe.

References

[1] V.A. Jerez, C.B. de Araújo, Y. Messaddeq, J. Appl. Phys. 96 (2004) 2530.
[2] M.J. Digonnet (Ed.), Rare Earth Doped Fiber Lasers and Amplifiers, Dekker, New York, , 1993.
[3] N.O. Dantas, F. Qu, Physica B 327 (2003) 79.
[4] T. Hayakawa, M. Nogam, J. Appl. Phys. 90 (2001) 2200.
[5] B. Peng, X.M. Qiu, L. Jiang, Z.C. Fan, W. Huang, Appl. Phys. Lett. 85 (2004) 1910.
[6] S.X. Dai, J.J. Zhang, S.G. Li, J.H. Yang, S.Q. Xu, G.N. Wang, L.L. Hu, J. Mater. Sci. Technol. 20 (2004) 668.
[7] I.V. Kityk, J. Wasylak, D. Dorosh, J. Kucharski, D. Dorosz, A. Brenier., Mater. Lett. 49 (2001) 272.
[8] B.R. Judd, Phys. Rev. 127 (1962) 750.
[9] G.S. Ofelt, J. Chem. Phys. 37 (1962) 511.
[10] Hong Li, Liyu Li, Denis M. Strachan, Maoxu Qian, J. Non-Cryst. Solids 349 (2004) 127.
[11] Y. Nageno, H. Takebe, K. Morinaga, J. Am. Ceram. Soc. 76 (1993) 3081.
[12] H. Takebe, Y. Nageno, K. Morinaga, J. Am. Ceram. Soc. 77 (1994) 2132.
[13] E.W.J.L. Oomen, A.M.A. van Dongen, J. Non-Cryst. Solids 111 (1989) 205.
[14] K. Gatterer, Borate glasses, in: A.C. Wright, S.A. Feller, A.C. Hannon (Eds.), Proceedings of the 2nd International Conference on Borates, Crystals and Melts, Society of Glass Technology, , 1997, p. 384.
[15] K. Gatterer, G. Pucker, W. Jantscher, H.F. Fritzer, S. Arafa, J. Non-Cryst. Solids 176 (1998) 189.
[16] S. Tanabe, T. Hanada, T. Ohyagi, N. Soga, Phys. Rev. B 48 (1993) 10591.
[17] S. Tanabe, J. Non-Cryst. Solids 259 (1999) 1.
[18] W.T. Carnall, P.R. Fields, K. Rajnak, J. Chem. Phys. 49 (1968) 4424.
[19] W.T. Carnall, P.R. Fields, B.G. Wybourne, J. Chem. Phys. 42 (1965) 3797.
[20] K.B. Yatsimirskii, N.K. Davidenko, Coord. Chem. Rev. 271 (1979) 223.
[21] W.E.F. Ayta, V.A. Silva, N.O. Dantas, J. Lumin. 130 (2010) 1032.
[22] D. Manara, A. Grandjean, D.R. Neuville, Am. Mineral. 94 (2009) 777.
[23] A.A. El-Kheshen, F.H. El-Batal, S.Y. Marzouk, Ind. J. Pure Appl. Phys. 46 (2008) 225.
[24] H. Aguiar, E.L. Solla, J. Serra, P. Gonzalez, B. Leon, N. Almeida, S. Cachinho, E.J.C. Davim, R. Correia, J.M. Oliveira, M.H.V. Rernandes, J. Non-Cryst. Solids 354 (2008) 4075.
[25] J.B. Bates, J. Chem. Phys. 57 (1972) 4042.
[26] S.A. Lourenço, N.O. Dantas , E.O. Serqueira , W.E.F. Ayta , A.A. Andrade , M.C. Filadelpho, J.A. Sampaio, M.J.V. Bell, M.A. Pereira-da-Silva, J. Lumin., in press, doi:10.1016/j.jlumin.2010.11.028.
[27] F. Ramos, H. Loro, E. Camarillo, J. García Solé, A.A. Kaminskii, U.G. Caldiño, Opt. Mater. 12 (1999) 93.
[28] Dwight R. Jennison, A.Barry Kunz, Phys. Rev. B 13 (1976) 5597.
[29] A.J.G. Ellison, P. Hess, J. Geophys. Res. 95 (1990) 15717.
[30] C.K. Jorgensen, R. Reisfeld, J. Less-Common Met. 93 (1983) 107.
[31] M. Abril, J. Méndez-Ramos, I.R. Martín, U.R. Rodríguez-Mendoza, V. Lavín, A. Delgado-Torres, V.D. Rodríguez, P. Núñez, A.D. Lozano-Gorrín, J. Appl. Phys. 95 (2004) 5271.
[32] R.R. Jacobs, M.J. Weber, J. IEEE, Quant. Electron. 12 (1976) 102.
[33] M. Ajroud, M. Haouari, H. Ben Ouada, H. Maaref, A. Breniert, C. Garapon, J. Phys.: Condens. Matter 12 (2000) 3181.
[34] I.R. Martín, Y. Guyot, M.F. Joubert, R.Yu. Abdulsabirov, S.L. Korableva, V.V. Semashko, J. Alloys Compd. 323–324 (2001) 763.
[35] R.R. Jacobs, M.J. Weber, IEEE J. Quant. Electron. QE 12 (1976) 102.
[36] A.A. Kaminskii, Laser Crystals: Their Physics and Properties, Springer, New York, 1989.